C. R. Physique 14 (2013) 94–105

Contents lists available at SciVerse ScienceDirect

Comptes Rendus Physique

www.sciencedirect.com

Physics in High Magnetic Fields / Physique en champ magnétique intense

Iron-based superconductors in high magnetic fields

Supraconducteurs à base de fer en champ magnétique intense

Amalia I. Coldea [a,*], Daniel Braithwaite [b], Antony Carrington [c]

[a] *Clarendon Laboratory, Department of Physics, University of Oxford, Parks Road, Oxford OX1 3PU, UK*
[b] *SPSMS, UMR-E CEA / UJF-Grenoble, INAC, 38054 Grenoble, France*
[c] *H.H. Wills Physics Laboratory, University of Bristol, Tyndall Avenue, Bristol BS8 1TL, UK*

ARTICLE INFO

Article history:
Available online 20 September 2012

Keywords:
Superconductivity
High magnetic fields
Iron-based superconductors
Upper critical field
Quantum oscillations

Mots-clés :
Supraconductivité
Fort champ magnétique
Supraconducteurs à base de fer
Champ critique supérieur
Oscillations quantiques

ABSTRACT

Here we review measurements of the normal and superconducting state properties of iron-based superconductors using high magnetic fields. We discuss the various physical mechanisms that limit superconductivity in high fields, and the information on the superconducting state that can be extracted from the upper critical field, but also how thermal fluctuations affect its determination by resistivity and specific heat measurements. We also discuss measurements of the normal state electronic structure focusing on measurement of quantum oscillations, particularly the de Haas–van Alphen effect. These results have determined very accurately, the topology of the Fermi surface and the quasi-particle masses in a number of different iron-based superconductors, from the 1111, 122 and 111 families.

RÉSUMÉ

Nous passons en revue les mesures en fort champ magnétique des propriétés normales et supraconductrices des nouveaux composés supraconducteurs à base de fer. Nous rappelons les mécanismes qui limitent la supraconductivité à haut champ et discutons les informations sur la phase supraconductrice qui sont obtenues grâce à la mesure du champ critique supérieur, mais également les effets des fluctuations thermiques sur la détermination de celui-ci par des mesures de transport ou de chaleur spécifique. Nous discutons également la structure électronique de la phase normale, principalement par des mesures d'oscillations quantiques comme l'effet de Haas–van Alphen. Ces résultats permettent de déterminer très précisément la topologie de la surface de Fermi et la masse des quasi-particules dans plusieurs supraconducteurs à base de fer des familles 1111, 122 et 111.

1. Introduction

This short review summarizes research on iron-based superconductors made using high magnetic fields since their discovery in 2008. Here we mainly review studies of the normal state electronic structure (Fermi surface and transport

* Corresponding author.
E-mail addresses: amalia.coldea@physics.ox.ac.uk (A.I. Coldea), daniel.braithwaite@cea.fr (D. Braithwaite), a.carrington@bristol.ac.uk (A. Carrington).

1631-0705/$ – see front matter
http://dx.doi.org/10.1016/j.crhy.2012.07.003

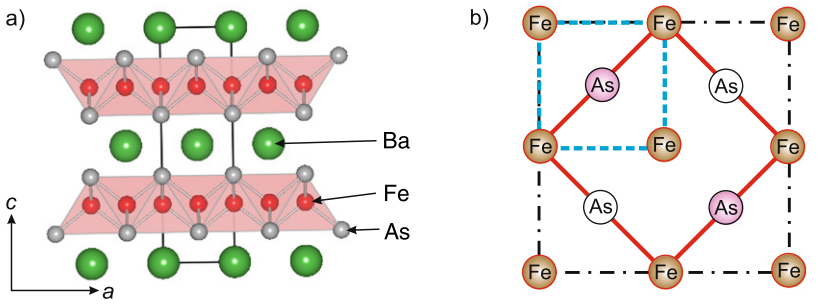

Fig. 1. Crystal structure of iron-based superconductors: (a) In the a–c plane for a 122-type FeBS ($BaFe_2As_2$), showing the conducting FeAs layer separated by the Ba atom; (b) Structure of the Fe–As plane. The As atom is either above (filled circles) or below (empty circles) the Fe plane. The dashed line shows the 1 Fe atom unit cell which would be the crystallographic one if the As atoms could be ignored. The solid line denotes the actually crystallographic unit cell which contains 2 Fe atoms. In the antiferromagnetic SDW state the cell further doubles to contain 4 Fe atoms (dot-dashed line). This is accompanied by a slight orthorhombic distortion.

properties) and studies of the superconducting state – particularly the behaviour of the upper critical field (H_{c2}). In the main, we will focus on experiments which are close to our own research interests (electrical transport, specific heat and quantum oscillations). We begin with a brief description of the essential properties of these materials before describing in more detail some of the high field experiments.

1.1. Iron-based superconductors

There are now known to be several different families of iron-based superconductor (FeBS). The subject actually began in 2006 with the discovery of superconductivity at low temperatures in LaFePO [1], however worldwide interest took off when the first compounds with T_c up to 55 K were discovered in the $RFeAs(O_{1-x}F_x)$ (R = La, Ce, Pr, Sm, Nd) series [2,3]. These are known as the 1111 compounds because of the ratio of the constituents of the parent compound (without F). The T_c values for this family are the highest so far discovered for FeBS. However, to date the most highly studied materials are the 122 compounds XFe_2As_2 (X = Ca, Sr, Ba, K). In particular, $BaFe_2As_2$ has been found to a highly versatile parent, as superconductivity may be induced by hole doping with K on the Ba site [4], electron doping with Co on the Fe site [5] or isoelectric substitution of As with P [6] or Fe with Ru [7]. Superconductivity can also be induced by pressure [8]. A generic phase diagram is shown in Fig. 2. In general, all these substitutions weaken the antiferromagnetic ordering (decrease T_N) of the parent material and induce a dome of superconductivity, the maximum T_c of which seems to coincide with the extrapolated end point of the antiferromagnetic phase. Such a point is known as a quantum critical point as the fluctuations between the phases on either side of this point at zero temperature are driven by quantum as opposed to classical thermal fluctuations [9]. To the left of the quantum critical point there is evidence that, in many of the materials, antiferromagnetic order coexists microscopically with superconductivity.

In addition to these two families there are also the 111 materials (LiFeAs and LiFeP) and the 11 material FeSe/Te. The 111 materials are so far unique in that both the As and P sister compounds are not magnetically ordered and both superconduct, with T_c of 17 K [10,11] and 4 K [12] respectively. The 11 material is different in that it does not contain a group 15 (pnictogen) element (As or P) but rather one from group 16, the chalcogenides Se or Te. The maximum T_c in the 11 materials can be quite high, increasing up to ∼37 K under pressure [13].

The structural element which is common to all the FeBS is a square planar Fe layer, as shown in Fig. 1. In the centre of each Fe square sits a pnictogen or chalcogen element, forming a tetrahedral shape. The pnictogen/chalcogen atom sits alternately above or below the Fe plane in adjacent Fe squares, making the crystallographic unit cell $\sqrt{2}$ larger than it otherwise would be (see Fig. 1). The above is not an exhaustive list and new materials are still being discovered.

1.2. Band-structure and superconductivity

The ubiquitous square planar Fe layer in the FeBS leads to them all having distinctive similarities in their electronic structure. The undoped parent materials are compensated semi-metals meaning that they have equal numbers of electrons and holes. In their paramagnetic state the hole and electron Fermi surfaces are quasi-two-dimensional and are centred in the middle and the corner of the Brillouin zone, respectively (as shown for different compounds in Figs. 4–6). There are typically either 2 or 3 hole sheets and 2 electron sheets which are of similar size and shape and are therefore quasi-nested. This means that translation of the hole sheets by the vector, $Q_0 = (\pi/a, \pi/a)$, almost causes them to coincide with the electron sheets, as shown for LaFePO in Fig. 2. This property causes a peak in the generalized susceptibility $\chi(Q)$ at this Q vector and when not magnetic ordered, strong spin fluctuations are expected with a spread of Q values centred at Q_0. The magnetism itself is likely driven by strong intra orbital Hund's coupling producing a large local moment on each Fe atom rather than a Peierls like nesting driven instability [15].

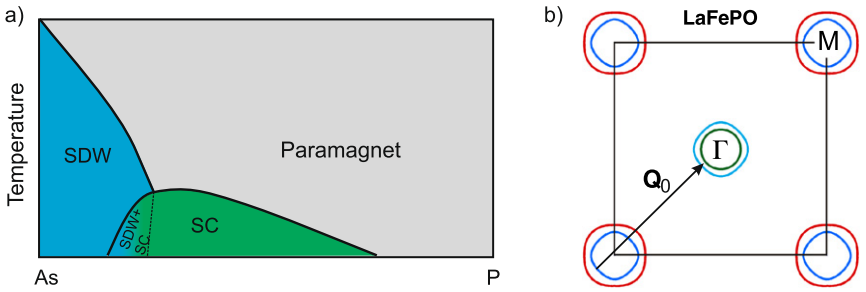

Fig. 2. (a) A generic phase diagram of the iron-based superconductors. The horizontal axis here denotes the changes as a function of composition in the $BaFe_2(As_{1-x}P_x)_2$ series, but very similar diagrams are obtained as a function of electron or hole doping or as a function of external pressure. (b) Fermi surface slice at the centre of the Brillouin zone (Γ point) for LaFePO showing the nesting vector, Q_0, between the inner electron and hole bands that have the same orbital character (after Ref. [14]).

The combination of $Q = Q_0$ spin-fluctuations and the quasi-nested electron–hole quasi-two-dimensional Fermi surfaces in FeBS are thought to lead to a highly unusual pairing state, where the superconducting gap has the opposite sign on the electron and hole sheets [16–19]. In the simplest case theoretical models suggest that the gap has no nodes but nodes may appear either when the (spin fluctuation) scattering between the electron sheets is strong compared to the electron–hole scattering or due to strong c-axis warping of some hole sheets [20–23]. Experimentally there is strong evidence for both nodal and nodeless pairing states in *different* FeBS, and it is likely that these differences are intimately tied to the structure of the Fermi surface in the particular materials [24,25].

2. Superconducting state – probes of H_{c2}

2.1. High field phase diagram of the Fe superconductors

The determination of the upper critical field (H_{c2}) of the FeBS is an essential aspect of the experimental effort on these systems. The capability of superconductivity to survive in high fields is of course one of the important factors for future applications using high-T_c superconductors. But mainly, the precise knowledge of the temperature dependence of H_{c2} is an important tool for revealing the thermodynamic parameters and the microscopic mechanisms of these unconventional superconductors. The first indication of the condensation energy of the superconducting state is the critical temperature: in general high T_c leads to high H_{c2} (in BCS theory, $H_{c2} \sim T_c^2$). This is true in the FeBS, as most of the reported values for H_{c2} for FeBS with T_c in the range 30–40 K lie in the range 30–70 T. These values mean that some of these materials could be good candidates for high field applications as recently detailed by Putti et al. [29]. The other significant aspect of these field values is that while they are beyond the reach of most laboratories, a large part of the phase diagram can be explored in the static magnetic field available in high field facilities, and indeed the whole phase diagram in many systems is accessible using state of the art pulsed field techniques.

An external magnetic field induces pair-breaking through two mechanisms. The orbital mechanism is due to the effect of the field on the Cooper pairs, and depends on the coherence length, so giving an indication of the effective mass. Because the coherence length diverges at the critical temperature, H_{c2} close to T_c is always governed by the orbital limit, and the slope dH_{c2}/dT at T_c (H'_{c2}) is the relevant parameter to obtain this information. The other mechanism is the paramagnetic or Pauli pair-breaking due to the Zeeman energy of the external field on the spins of the electrons forming the pairs. The temperature dependence of H_{c2} including both contributions must be solved numerically, as first done by Werthamer, Helfand and Hohenberg (WHH) [30]. To the simple model of weak coupling in the clean limit several refinements can be added: reduced mean free path (dirty limit), strong coupling effects, and multiband superconductivity. Measurements in high fields have now been performed on many different FeBS. The general aspect of the H_{c2} diagram shares certain characteristics for all of them as can be seen in Fig. 3. The slope at T_c is steeper for $H \| ab$ than for $H \| c$ with fairly modest effective mass anisotropy. This anisotropy of H_{c2} tends to decrease towards lower temperatures. An unconventional temperature dependence (either rather linear or with positive curvature) is often found for $H \| c$ and the low temperature values of H_{c2} often significantly exceed the BCS Pauli limit of $1.84T_c$.

2.2. Flux dynamics

Before developing the above points, a word of warning. Most of the experimental determinations of H_{c2} are done by electrical transport techniques. Flux flow can generate resistance within the superconducting state, and experience with the cuprates has shown that this can be particularly important at high temperature. Transport measurements tend to reveal the 'irreversibility line' which corresponds to a transition or crossover between a vortex lattice to a vortex liquid. This may be quite different to the thermodynamic H_{c2}. Ideally, transport measurements should always be compared with a thermodynamic probe such as specific heat. To date there are relatively few studies of H_{c2} determined from specific heat, especially at high field. The phase diagram in magnetic field has been determined by specific heat at low fields (less than

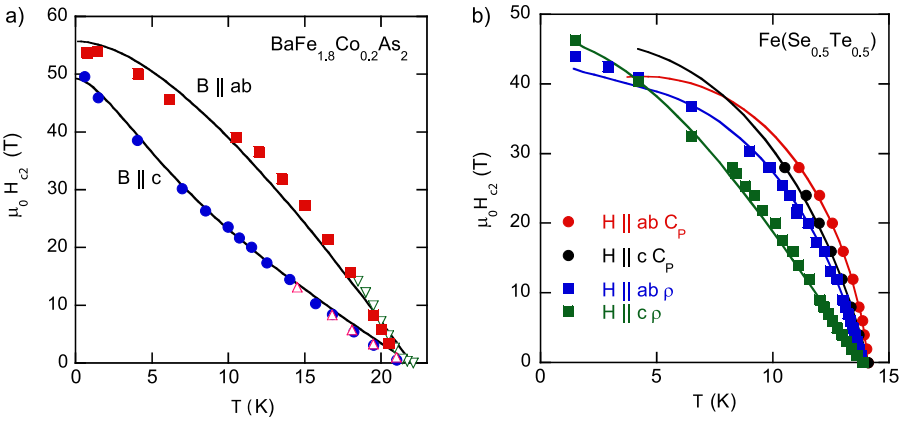

Fig. 3. (a) The determination of H_{c2} from resistivity measurements in $BaFe_{1.8}Co_{0.2}As_2$. The data were collected in pulsed field (solid symbols) and dc field (open symbols). The solid lines are fits to a two-band model. Adapted from Ref. [26]. (b) Comparison of H_{c2} determined from resistivity (squares) and specific heat (circles) of a single crystal of the $FeSe_{0.5}Te_{0.5}$. The solid lines are fits with a one band strong coupling model. Interestingly although the phase diagram is quite different when determined from specific heat, the crossing of the lines for $H\|c$ and $H\|ab$ found from the transport data is still predicted (adapted from Refs. [27,28]).

10 T) in several systems. In the 1111 compound $NdFeAsO_{1-x}F_x$ Welp et al. [31] reported initial slopes (H'_{c2}) of 3.1 T/K for $H\|ab$ and 0.7 T/K for $H\|c$. Putti et al. [29] actually report higher slopes from transport data (10 T/K and 2 T/K) though point out that the transition broadens considerably and use an onset criterion. Pribulova et al. [32] compared specific heat and torque measurements on the same 1111 system and reveal an extended area corresponding to a vortex liquid. The 122 compound $(Ba,K)Fe_2As_2$ is probably the most studied Fe superconductor, and is also one of the cleanest systems. In this compound Welp et al. [33] reported H'_{c2} values of 17.5 T/K ($H\|ab$) and 6.5 T/K ($H\|c$) from specific heat data. These values are considerably higher than all the results obtained from transport data which find slopes of the order of 5 T/K for $H\|ab$ and 2.5 T/K ($H\|c$) [34,29]. For the 11 system Fe(Se,Te) two groups showed by measurements on single crystals with similar compositions that at low fields the H_{c2} line determined from transport data was considerably lower than that determined from specific heat [27,28,35]. Specific heat measurements at low fields are sufficient to show that there is a difference between specific heat and transport, but in order to obtain the full thermodynamic phase diagram measurements at higher fields are necessary. So far Fe(Se,Te) is the only system where specific heat measurements have been carried out at much higher fields [28] with recently developed high field relaxation and temperature modulated specific heat measurements. It therefore appears that in all reported cases there are considerable differences between the H_{c2} line determined from transport and specific heat measurements. Caution should therefore used when interpreting in detail the phase diagrams that have been determined only from resistivity measurements. A considerably more significant effort to determine the phase diagrams at high field is clearly extremely desirable. Measurements in very high static field are now available. Recently, the feasibility of temperature modulated calorimetry measurements in pulsed field has also been shown [36], and this technique undoubtedly holds much promise for the future.

2.3. Pauli limiting

An important aspect is to determine whether Pauli limiting plays a role for H_{c2}. If Pauli limiting is completely absent it may suggest that the order parameter is p-wave. The first analysis of H_{c2} in the 1111 system [37] found that H_{c2} exceeded the BCS paramagnetic limit and that the temperature dependence could be explained with a two-band model and only orbital limiting. However, shortly afterwards, Fuchs et al. [38] also measuring the 1111 family suggested that Pauli limiting should be included. Similarly, in the 122 family, while most studies included Pauli limiting to fit the H_{c2} curves, some found that it was unnecessary [39,40]. These uncertainties stemmed from at least two reasons. Firstly, the experimental values of H_{c2} do in several cases significantly exceed the theoretical Pauli limit for a BCS superconductor [37,39]. However, this is not proof that Pauli limiting does not play a role as other effects such as strong coupling can enhance the Pauli limit. Secondly, these systems are relatively weakly correlated, the low temperature orbital limit ($0.69\ T_c\ H'_{c2}$ in the WHH model) exceeds the theoretical Pauli limit but not hugely. Therefore, the influence of Pauli limiting even if present is not strong. Obviously the absence of apparent Pauli limiting is only significant if the orbital limit exceeds the Pauli limit. The situation became much clearer in the 11 Fe(Se,Te) system. This system seems to have much stronger correlations [41]. In Fe(Se,Te) several studies have determined H_{c2} up to high field and in all cases clear Pauli limiting is seen [27,42,28,43]. Pauli limiting has also been found for the 111 system LiFeAs [44]. It now seems to be established that Pauli limiting is present in most high T_c FeBS, implying almost certainly singlet pairing.

2.4. Anisotropy

The reported anisotropy for the effective mass inferred from the slope at T_c is not so weak and factors of 3–5 are generally found. The fact that this is often described as rather modest anisotropy is mainly in comparison with the cuprates, showing that these systems are clearly not 2D. The reported slopes of H_{c2} are large to extremely large. Taking the most reliable data obtained from specific heat measurements, for $H\|ab$ slopes of $H'_{c2} = 3$ T/K, 17 T/K and a huge 40 T/K have been reported for the 1111, 122, and 11 families respectively [31,33,28]. This implies rather small correlation lengths, of the order of 1 nm (0.4 nm in Fe(Te, Se)). An interesting and unusual aspect of all four families is that the anisotropy of H_{c2} decreases at low temperature. H_{c2} often becomes rather isotropic at low temperature, and in Fe(Te, Se) an inversion of the anisotropy was even found [27,35]. Of course, caution should be used here taking into account the previous paragraph on flux dynamics. However, in the only case where the phase diagram has been established from specific heat measurements up to 28 T this reduction of the anisotropy was confirmed, and a fit of the curves to a simple model even predicts the crossing of the curves at lower temperature as seen in the transport data [28]. Except in certain very special cases, the Pauli limiting mechanism should be almost isotropic, but an isotropic Pauli limit does not imply necessarily an isotropic H_{c2} at low temperature [27]. In fact in Fe(Te, Se) a large (and rather unrealistic) anisotropy of 4 was required for the Pauli limit to fit the H_{c2} curves obtained from resistivity measurements with a simple model. This is probably the case in other systems too, and may be avoided using two-band models (see below). However when the thermodynamic H_{c2} line obtained from specific heat was used it was found that the curves could be fitted with a simple model and a reasonable (20%) anisotropy of the Pauli limiting mechanism.

2.5. Positive curvature and multi-band superconductivity

The unusual temperature dependence of H_{c2} for $H\|c$, showing either positive curvature or at least an almost linear behaviour led to several groups fitting this temperature dependence with a two-band or two-gap superconducting model. Indeed, this behaviour is similar to that found in MgB_2 where the multigap character of superconductivity is well established now. A two-band model has been used for the 1111 family [37], for the 122 systems [39,26,42,45] and for the 111 system [44]. Fitting using a two-band model introduces many extra parameters. The main ones are the Fermi velocities of the two bands, to which are added the intra-band coupling constant for each band, and the interband coupling between the bands. It is extremely likely that there are at least two bands, probably more, contributing to superconductivity in the FeBS. Whether this induces sufficiently different gaps for the two-gap model to be applied is still an open question. In order to reproduce the experimental curves the fits tend to need a rather large ratio between the Fermi velocities of the two bands (typically more than 10). To our knowledge no theoretical or other experimental findings support such a large ratio. But perhaps more importantly in Fe(Se, Te), the only case where the thermodynamic H_{c2} has been measured by specific heat up to high fields only one band approach seems to be sufficient, whereas from the transport data a two-band model fits the data better [27]. Behind the use of a two-band model in the FeBS is the idea that the two bands could correspond to the electron and hole Fermi surface pockets. Of course, most superconductors have multiple energy bands crossing the Fermi surface but those where distinct gaps exist on the different sheets are quite rare. The reason is that scattering generally mixes the k-states in the different bands so that any intrinsic anisotropy in the pairing potential gets averaged out, but in some cases the scattering is sufficiently selective that this does not occur. To what extent this occurs in the FeBS is still to some extent an open question but multiple gaps have been widely used to explain for example, specific heat, magnetic penetration depth and angle resolved photoemission (ARPES) data. In some cases it could be however, that the second gap is really just a sub-band created by impurity scattering rather than a distinct gap on a second sheet. It is difficult to distinguish these two possibilities from bulk properties and ARPES can suffer from surface effects so that the measured gaps might not be representative of the bulk. However, consistency between the different probes should help establish the correct gap structure and measurements of H_{c2} up to high fields certainly has a part to play.

3. Normal state – probes of the electronic structure

High magnetic fields are used in a variety of different ways to investigate the normal state behaviour of superconductors. One key aspect is that often a large field is needed to suppress the superconductivity so that the normal state may be accessed. There are a number of different measurements which then give access to the electronic properties. The most commonly used are the $\boldsymbol{k}$-integrated transport probes such as the electric resistance (magnetoresistance and Hall effect) and the electro-thermal responses [Seebeck, Nernst, Ettingshausen, Reghi-Leduc (thermal Hall) effects]. These semi-classical effects are sensitive to both the Fermi surface geometry and the energy and $\boldsymbol{k}$ dependence of the scattering rates, although disentangling the relevant parameters can be somewhat model dependent.

By changing the angle of the magnetic field with respect to the crystal axes, it is possible to extract $\boldsymbol{k}$-resolved information in some cases. Most notable in this regard is field angle dependent magnetoresistance (ADMR) which has been used with great effect to determine the Fermi surface and anisotropy and temperature dependence of the scattering rate in the overdoped cuprate superconductor $Tl_2Ba_2CuO_{6+\delta}$ [46–48], organic superconductors [49] and recently the iron-based superconductor, KFe_2As_2 [50]. The effect is most easily interpreted in quasi-two-dimensional systems which are dominated by a small number of Fermi surface sheets. Measurements of the c-axis (low conducting direction) resistance are measured

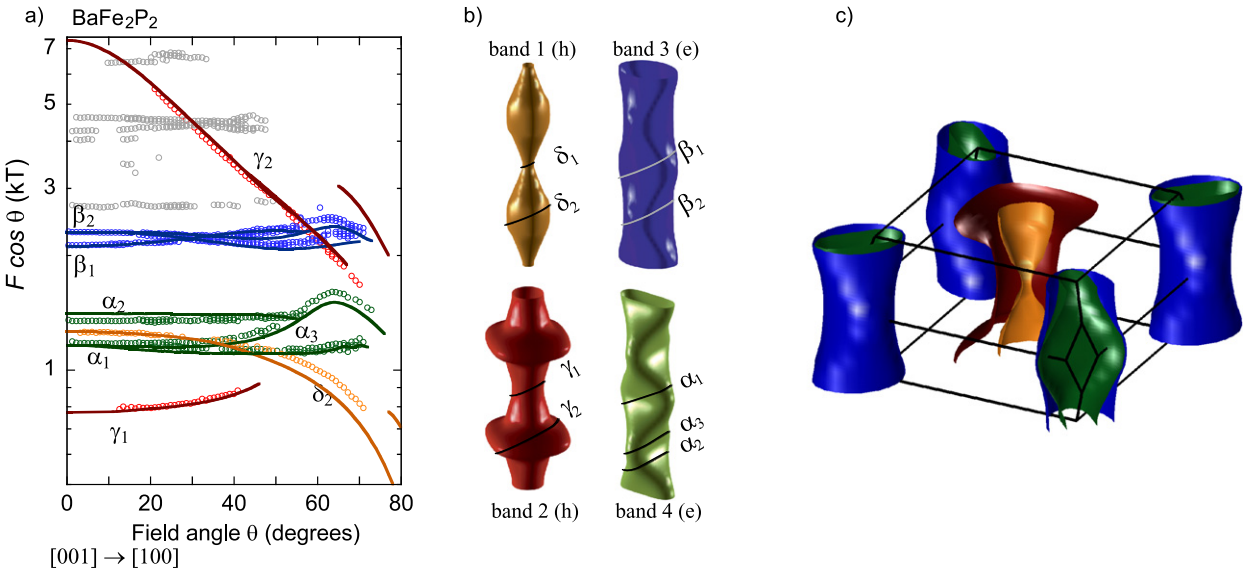

Fig. 4. (a) Experimentally measured de Haas–van Alphen frequencies for $BaFe_2P_2$ (symbols), along with the orbits from the band structure calculations (solid lines). The band energies found in the DFT calculations have been shifted to bring the predicted surface in line with experiment. For the hole band 1 the shift was −113 meV, whereas for electron bands 3 and 4 the shifts were +58 and +68 meV respectively. For band 2 a shift proportional to the d_z^2 character was applied so that at the middle of the band (Γ–X plane) the shift was −52 meV whereas at the top of the zone (where the surface has strong warping and d_{z^2} character the shift was close to zero [52]). (b) The origin of the extremal orbits is indicated on the various Fermi surface sheets. (c) The complete Fermi surface of $BaFe_2P_2$ (after Ref. [53]).

as the magnetic field is rotated in both the polar (θ) and azimuthal directions (ϕ). The electrons perform (partial) orbits of the Fermi surface in planes perpendicular to the field and this orbital motion effects the c-axis resistance. In the simple case where there is a single Fermi surface with weak cosine warping, at certain angles the c-axis component of the Fermi velocity average to zero over an orbit and hence there is a pronounced maximum in the magneto-resistance at this angle. The angles where this occurs are periodic and the characteristic oscillations in ρ_c as a function of θ are known as Yamaji angle dependent magneto resistance oscillations (AMRO) [51].

Although ADMR and AMRO are undoubtedly powerful techniques their applicability is practically limited to materials which have one or two sheets of almost two-dimensional Fermi surface. A more generally applicable technique is the phenomena of magneto quantum oscillations (QO). Unlike the aforementioned techniques, quantum oscillations are a truly quantum phenomenon in that their existence relies on the Landau quantization of energy levels in a field. In order to observe the effect an appreciable amount of the electrons need complete a cyclotron orbit before they are scattered by impurities. Several other factors can also damp the QO signal – such as finite temperature, imperfect crystallinity, and superconductivity, so experiments need to be performed on very high quality samples at low temperatures (generally below 4 K) and in very high magnetic fields.

3.1. Magneto-quantum oscillations

As the size of the electron Landau orbits increase along with the magnetic field they periodically pass through the Fermi level giving an abrupt change in their occupancy and an associated jump in the free energy. This gives rise to periodic (in inverse field) changes in most physical quantities but the most commonly measured are the magnetization/torque or the resistivity which are known as the de Haas–van Alphen effect and the Shubnikov–de Haas effect respectively. The power of the techniques is that the frequency of the oscillations is directly proportional to the ***k***-space area of the orbits. Normally, only the extremal orbits of the Fermi surface contribute and so there are only a small number of observed oscillation frequencies which are easily separated by Fourier transforming the measured signal.

Compared to the competitive technique of ARPES, the QO technique has several advantages but also a few disadvantages. The main advantage is that it is unambiguously a bulk probe. In synchrotron-based ARPES the escape depth of the electron is typically only 3–5 Å which is less than half of the c-axis lattice parameter so there is often ambiguity as to whether the bands measured are bulk or surface and also *if* they are of bulk origin whether the bands are modified from those in the bulk. A further advantage is that the QO technique can measure the full three-dimensional structure of the Fermi surface with very high resolution (typically the noise level corresponds to an area which is ∼0.05% of the Brillouin zone cross-section). Although ARPES can also measure the k_z dispersion, by varying the photon energy, its resolution is relatively limited (typically 10–30% of c^*) because of the short escape depth – although this can be improved with lower photon energy laser-based ARPES where the escape depth is much longer. The main problems with the QO technique are that very pure samples and low temperatures are required so that many doped system are not measurable nor are states which occur

only at high temperatures such as the paramagnetic state of the arsenide parent materials of the FeBS. Finally, QO does not give unambiguous information about where an orbit originates on the Fermi surface. Typically this can only be achieved by comparison to band-structure calculations and in cases where several orbits have similar sizes, which is relatively common in FeBS where there is quasi-nesting of the electron and hole Fermi surfaces, very high resolution (large $1/B$ space) is needed to separate them. The use of high magnetic field is an necessity for these measurements for three reasons: first to reduce the cyclotron radius of the electrons and thus increase the chances of them completing an orbit before being scattered, second to quench the superconductivity which would otherwise gap the Fermi surface and strongly damp the QO signal, and third to increase the size of the $1/B$ measurement space and therefore improve resolution. It should be noted here that the Fermi surfaces areas measured in a QO experiment are normally always the zero field ones as long as the splitting of the up/down spin state energies are linear in field, as they are for a normal paramagnet.

There have now been measurements of QO on a large number of different FeBS and associated parent materials. In general, the observed Fermi surfaces are in good overall agreement with density functional theory (DFT) band structure calculations but there are a number of important differences which have implications for microscopic models of the superconductivity. There are generally two types of parent materials. The phosphorous containing materials generally have Fermi surfaces similar to the superconducting compounds mentioned in the introduction. However, the pure 1111 and 122 arsenides are spin density wave antiferromagnets at low temperature and have quite different Fermi surfaces to the paramagnetic materials mentioned above. The transition to the SDW state is accompanied by a structural distortion which, apart from a slight orthorhombicity, increases the size of the unit cell by $\sqrt{2}$ and rotates it by 45° compared to the paramagnetic state (see Fig. 1). To the first approximation this folds the electron and hole bands on top of one another. It might be expected then, that as these bands hybridize, there would be a gap formed where they cross, which because the pockets are approximately the same size, would occur at the Fermi level. This would wipe out the Fermi surface at these points leaving only small pockets where the cancelation has not occurred because of the slightly different size and warping of the sheets. In reality this simple picture is not quite correct because the bands shift significantly in energy as a result of the magnetism [56], however, the end result is the same in that small quasi three-dimensional pockets are expected.

QO measurements have been reported for all the 122 arsenides (XFe_2As_2 with X = Ba [57,58], Sr [59], Ca [60]) which have a SDW ground state, however the most complete data is for $BaFe_2As_2$. Here a small uniaxial stress was applied to detwin the sample [58]. This greatly increased the size of the SdH oscillations observed in the resistivity. Oscillations from all the Fermi surfaces expected from the DFT calculations were found. To get good agreement with the DFT calculation some small shifts to the calculated band energies were required. As we shall see it is often the case that the DFT calculations tend to overestimate the size of the pockets so to get agreement the electron bands need to be shifted up in energy and the hole and down. Here the shifts required were between 30 and 65 meV. These shift are likely due to dynamic many body effects not included in the DFT calculations such as on-site interactions, spin-fluctuations or phonons. For the same reasons the DFT calculations generally underestimate the effective mass. In a QO experiment the orbitally averaged mass may be determined by measuring the temperature dependence of the QO signal. Increasing temperature decreases the QO signal because the occupation of the Landau levels near the Fermi level is increasingly smeared as the temperature is increased. In $BaFe_2As_2$ the mass was found to be enhanced by between 1.7 and 3.6 depending on the orbit, compared to the DFT calculations. It is likely this increase is mostly due to the electron–electron interactions as the electron–phonon interaction is generally weak, giving only ∼20% increase in mass [61].

Complete determinations of the Fermi surfaces of the paramagnetic phosphorous parent 122 compounds (XFe_2P_2 with X = Ba [53], Sr [54], Ca [55]) have been made using dHvA oscillations of the torque produced by tiny samples (typically 20–100 μm in size) mounted on piezoresistive cantilevers designed for atomic force microscopy [62]. The small size of the highest purity samples makes this the preferred method for these materials. Experimental dHvA frequency versus field angle data for $BaFe_2P_2$ are shown in Fig. 4. Here, the frequency F has been multiplied by $\cos\theta$ on the vertical axis so as to highlight any departure of the data from two-dimensionality. For a perfect 2D cylinder $F \propto 1/\cos\theta$. A decrease in $F\cos\theta$ with increasing θ indicates that the cross-section decreases as k_z is changed from this local extrema, so the orbit is a local maxima, whereas an increase in $F\cos\theta$ indicates a local minima. All expected orbits (apart from the very small hole orbit δ_1) were observed over a large angular range. The DFT predictions are in excellent agreement over the measured angular once small band energy shifts are taken into account. The extent of the agreement gives us very high confidence that these shifted DFT calculations produce an excellent model of the Fermi surface topology. The band energy shifts reduce the size of both the electron and hole orbits and are between 50 and 110 meV. Interestingly, the size of the large hole orbit γ_2 is correctly predicted by the calculation without any shift. This is likely because it has different orbital character (d_{z^2}) to the others which are mostly $d_{xz/yz}$ and d_{xy} and has a markedly different size. These two facts mean that inter sheet spin-fluctuation scattering is likely suppressed for this section of Fermi surface, which supports the theory [63] that the band energy shifts are related to this scattering.

Data for $SrFe_2P_2$ [54] are quite similar to $BaFe_2P_2$ but those for $CaFe_2P_2$ are very different [55], as shown in Fig. 5. Here the smaller Ca ion reduces the spacing between the Fe layers and there is a dramatic (∼10%) reduction in c axis lattice parameter compared to Ba and Sr. This results in complete change in topology of the hole sheets which now form into a large pillow shaped surface centred on Z, as shown in Fig. 5. The observed frequencies associated with this sheet give stronger signals when the magnetic field is applied parallel to the ab plane, as shown in Fig. 5(c). The electron sheets merge and only a strongly warped electron cylinder is observed reflecting the significant interlayer coupling for systems

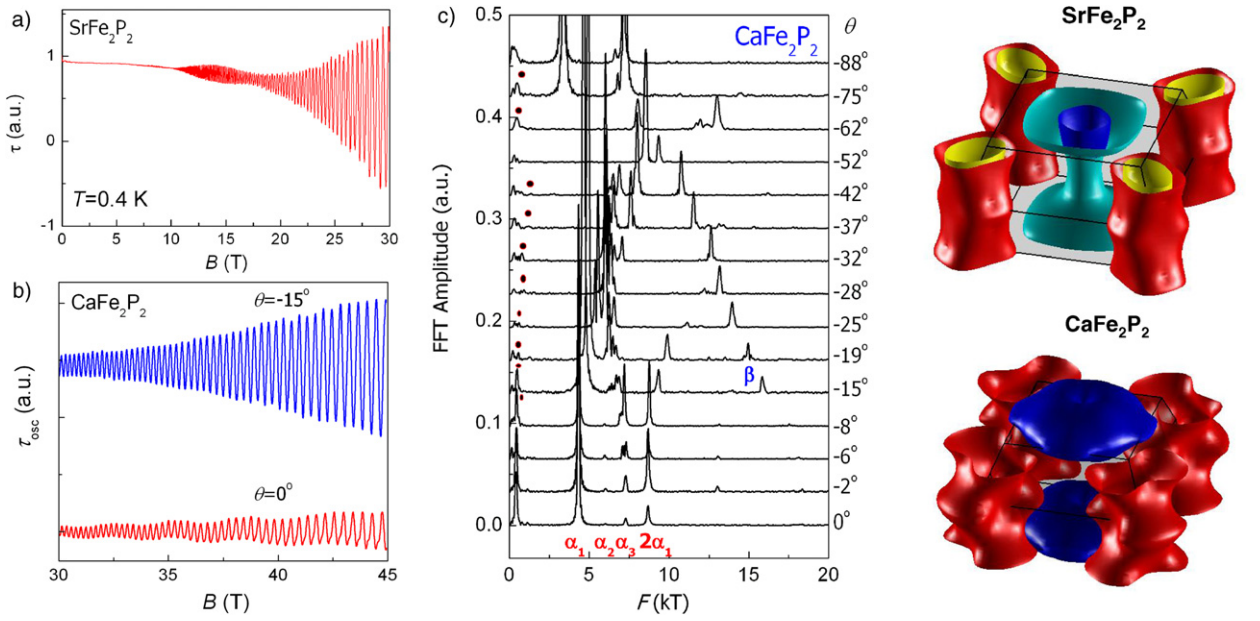

Fig. 5. (a) Torque data for $SrFe_2P_2$ up to 33 T and (b) $CaFe_2P_2$ up to 45 T. (c) The angular dependence of the Fourier transform spectrum that show the evolution of the measured dHvA frequencies versus field angle for the three-dimensional system, $CaFe_2P_2$ (where $(\theta = 0)$ corresponds to $B\|c$ rotating towards $B\|ab$); α orbits belong to the electron cylinder whereas the β orbit belongs to the 3D hole sheet. The Fermi surfaces of $SrFe_2P_2$ and $CaFe_2P_2$ as predicted by DFT calculations are also shown (after Refs. [54,55]).

with reduced c/a ratio [55]. The Fermi surface now lacks any degree of nesting and the DFT calculation predicts the correct topology without any appreciable band energy shifting.

Of course, the most interesting materials for study are the superconducting compositions. Normally, the scattering produced by introducing the dopant atoms needed to make the parent materials superconducting would mean that QOs would not be observable in available fields. However, there are fortunately a few important exceptions to this. Firstly, the relatively low T_c FeBS, LaFePO, LiFeAs and LiFeP superconduct without any doping and crystals with long mean-free-paths can be produced. For LaFePO, dHvA measurements [14,66] show that the largest signals are from the electron sheets but some small signals from the hole sheets are visible in the highest fields. Again to get agreement with the DFT calculations band energy shift between 50 and 100 meV were needed to reduce the size of the electron and hole sheets. The mass enhancement factors were found to be ~ 2.

The 11 compounds LiFeP and LiFeAs are of particular interest because unusually neither show any sign of magnetic order and both superconduct in their undoped state. In addition, magnetic penetration depth measurement show that LiFeP has a nodal gap structure whereas LiFeAs is nodeless [25]. The DFT calculations [67] suggest that both compounds have very similar Fermi surfaces, so explanations of the nodal-versus-nodeless gap structure being controlled by the presence or absence of a third d_{xy} hole sheet [22] (as proposed for the difference in behaviour of LaFePO (nodal) versus LaFeAsO (nodeless)) would seem unlikely to work here. Indeed as shown in Fig. 6 for LiFeP, dHvA oscillations from all the sheets predicted by DFT were observed [64] using pulsed fields up to 58 T and dc fields up to 45 T. A notable feature here is that LiFeP has three hole Fermi surface sheets, but the middle size one shows a much smaller mass enhancement that the other electron and hole sheets. This may indicate that the electron–hole scattering process is suppressed for this sheet (perhaps because of its orbital character rather than its shape) and that the pairing amplitude is weaker. This could make it an ideal place for node formation. For LiFeAs, clear dHvA signals were only observed for the electron sheets [64], however these were located very close to where DFT calculations predicted suggesting that the DFT accurately predicts the correct Fermi surface topology for this compound with minimal shifting. Very high mass renormalizations (up to $\sim$5) were found for LiFeAs compared to the smaller values ($\sim$3) for LiFeP, which are likely liked to the higher transition temperature in the former relative to the latter.

Finally we return to the 122 compounds to discuss $BaFe(As_{1-x}P_x)_2$ which is the only system discovered so far in which the changes in the Fermi surface can be tracked continuously using dHvA as material is tuned towards the quantum critical point where the superconductivity has the maximum T_c. The parent compounds $BaFe_2As_2$ and $BaFe_2P_2$ have already been discussed above. When P is substituted by As in this material, there is a remarkably small decrease in the electron mean free path on the electron pockets, and Shishido et al. [65] reported that dHvA oscillations from both electron sheets can still be seen up to $x = 0.41$ which corresponds to $T_c = 25$ K which is $\sim$80% of the maximum in this series (see Fig. 7). Signals from one of the hole sheets were also reported for a single composition ($x = 0.62$) by Analytis et al. [68], however, generally the scattering on the hole sheets is increased much more by the substitution. In Fig. 7 the changes in the electron sheet frequencies are shown. It can be seen that there is a monotonic decrease in the sheet size as the critical point is approached.

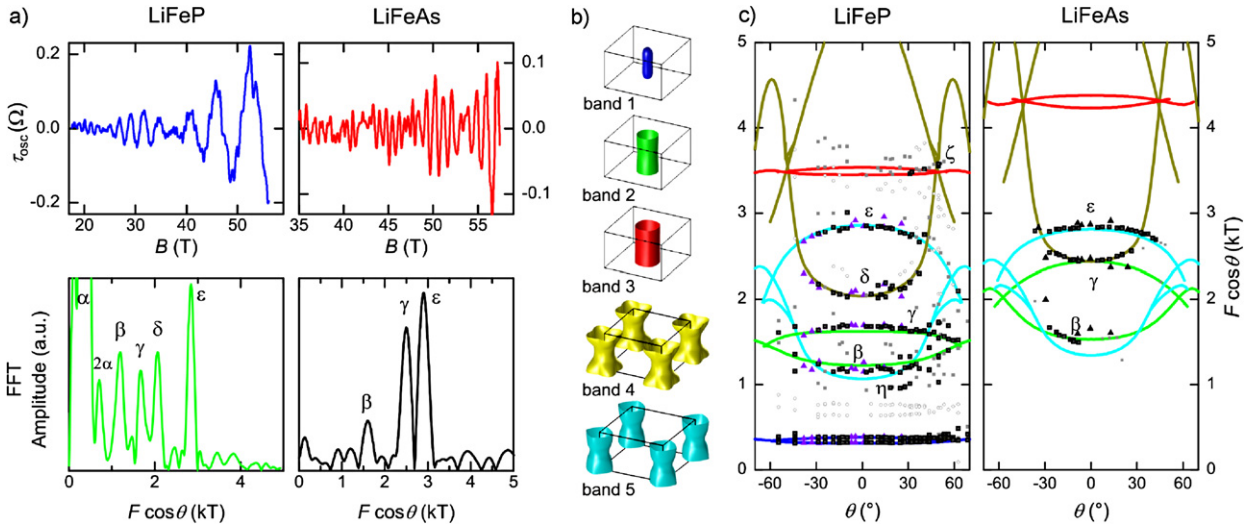

Fig. 6. (a) Raw dHvA data for LiFeP and LiFeAs in pulsed fields up to 58 T. The top panels show the raw data with smooth background subtracted and the bottom panels show the associated fast Fourier transforms with dHvA orbit peaks labelled. (b) Fermi surface sheets predicted by DFT calculations, band 1–3 are holes and 4, 5 are electrons. (c) The measured dHvA frequencies versus field angle for LiFeP and LiFeAs ($B \| c \equiv (\theta = 0)$ rotating towards the plane). Pulsed field data are shown as diamonds and the squares are dc field data. The solid lines are from the (shifted) DFT calculations. The small light squares have been identified as harmonics of the main frequencies. Figure adapted from Ref. [64].

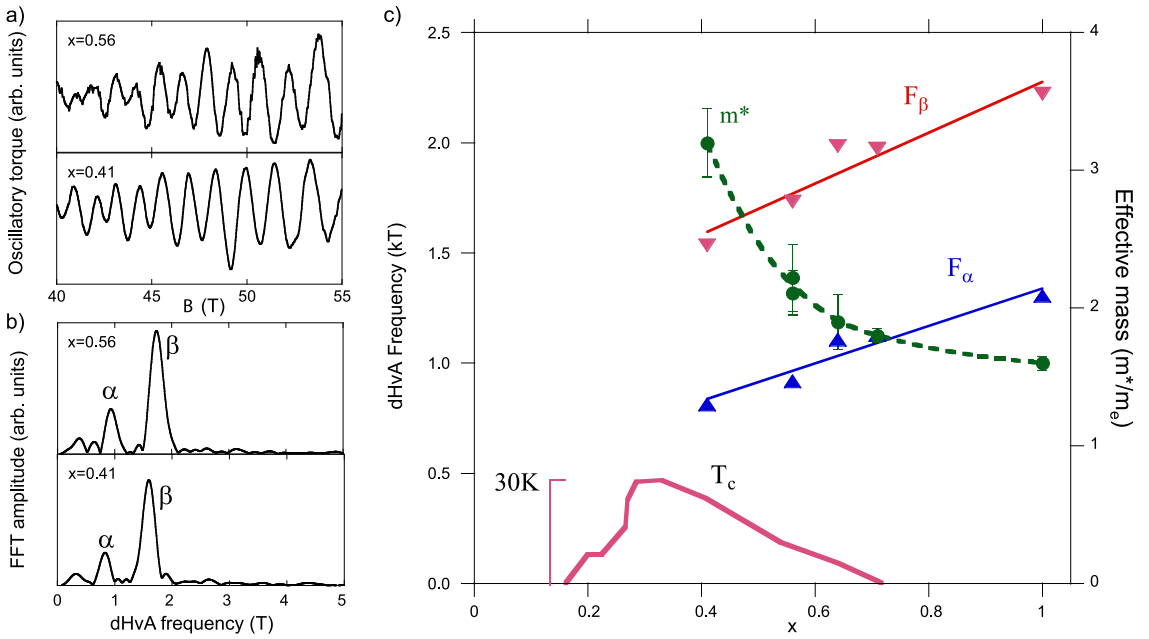

Fig. 7. (a) Raw torque data (with non-oscillatory background subtracted) for two compositions of $BaFe(As_{1-x}P_x)_2$, (b) FFT of the raw data in (a), (c) Average electron pocket frequency for both α and β sheets along with effective mass of the β sheet versus x. T_c versus x is also shown. Adapted from Ref. [65].

Such a decrease is not expected from DFT calculations so is likely a result of the increasing electron–electron correlations. At the same time there is a clear increase in the effective mass, reminiscent of the behaviour seen in some heavy Fermion compounds close to a quantum critical point [69]. For this material ARPES measurements of a close to optimal doping show consistent sized electron pockets and effective masses [70]. This is then perhaps the best example of the correlation induced Fermi sheet shrinking and effective mass enhancement driven presumably by the same correlation effect which cause high T_c superconductivity [63]. It remains a challenge to explain microscopically these observations but doing so could prove a powerful test of microscopic theories which seek to model the normal state electronic structure and superconductivity in these materials.

4. Concluding remarks

We have briefly reviewed the general characteristics of the iron-based superconductors and the contributions made by measurement in high magnetic field to determine the normal state electronic structure, the upper critical field and its anisotropy. This field is still quite young and the improved quality of the available crystals together with the discovery of new systems will help pave the way towards understanding the universality in behaviour between the different classes of compounds. However, it may be possible that besides the ingredients used so far by theory there are other aspects which need to be considered to account for all the observed phenomena and further measurements using high magnetic fields to understand the electronic structure of iron-based superconductors will be of great importance.

Acknowledgements

This work was partially supported by EPSRC (UK). We would like to acknowledge the support received while performing experiments at high magnetic field facilities in Europe (HFM-Nijmegen, LCMI-Toulouse/Grenoble) and the USA (NHMFL-Tallahassee).

References

[1] Y. Kamihara, H. Hiramatsu, M. Hirano, R. Kawamura, H. Yanagi, T. Kamiya, H. Hosono, Iron-based layered superconductor: LaOFeP, J. Amer. Chem. Soc. 128 (2006) 10012.
[2] Y. Kamihara, T. Watanabe, M. Hirano, H. Hosono, Iron-based layered superconductor $La[O_{1-x}F_x]FeAs$ ($x = 0.05$–0.12) with $T_c = 26$ K, J. Amer. Chem. Soc. 130 (2008) 3296–3297.
[3] R. Zhi-An, L. Wei, Y. Jie, Y. Wei, S. Xiao-Li, Zheng-Cai, C. Guang-Can, D. Xiao-Li, S. Li-Ling, Z. Fang, Z. Zhong-Xian, Superconductivity at 55 K in iron-based F-doped layered quaternary compound $Sm[O_{1-x}F_x]FeAs$, Chin. Phys. Lett. 25 (2008) 2215.
[4] M. Rotter, M. Tegel, D. Johrendt, Superconductivity at 38 K in the iron arsenide $(Ba_{1-x}K_x)Fe_2As_2$, Phys. Rev. Lett. 101 (2008) 107006.
[5] A.S. Sefat, R. Jin, M.A. McGuire, B.C. Sales, D.J. Singh, D. Mandrus, Superconductivity at 22 K in Co-doped $BaFe_2As_2$ crystals, Phys. Rev. Lett. 101 (2008) 117004.
[6] S. Jiang, H. Xing, G. Xuan, C. Wang, Z. Ren, C. Feng, J. Dai, Z. Xu, G. Cao, Superconductivity up to 30 K in the vicinity of the quantum critical point in $BaFe_2(As_{1-x}P_x)_2$, J. Phys. Condens. Matter. 21 (2009) 382203.
[7] S. Sharma, A. Bharathi, S. Chandra, V.R. Reddy, S. Paulraj, A.T. Satya, V.S. Sastry, A. Gupta, C.S. Sundar, Superconductivity in Ru-substituted polycrystalline $BaFe_{2-x}Ru_xAs_2$, Phys. Rev. B 81 (2010) 174512.
[8] P.L. Alireza, Y.T.C. Ko, J. Gillett, C.M. Petrone, J.M. Cole, G.G. Lonzarich, S.E. Sebastian, Superconductivity up to 29 K in $SrFe_2As_2$ and $BaFe_2As_2$ at high pressures, J. Phys. Condens. Matter. 21 (2009) 012208.
[9] S. Sachdev, B. Keimer, Quantum criticality, Phys. Today 64 (2011) 29–35.
[10] J.H. Tapp, Z.J. Tang, B. Lv, K. Sasmal, B. Lorenz, P.C.W. Chu, A.M. Guloy, LiFeAs: An intrinsic FeAs-based superconductor with $T_c = 18$ K, Phys. Rev. B 78 (2008) 060505.
[11] M.J. Pitcher, D.R. Parker, P. Adamson, S.J.C. Herkelrath, A.T. Boothroyd, R.M. Ibberson, M. Brunelli, S.J. Clarke, Structure and superconductivity of LiFeAs, Chem. Commun. 45 (2008) 5918.
[12] Z. Deng, X.C. Wang, Q.Q. Liu, S.J. Zhang, Y.X. Lv, J.L. Zhu, R.C. Yu, C.Q. Jin, A new "111" type iron pnictide superconductor LiFeP, EPL 87 (2009) 37004.
[13] S. Medvedev, T.M. McQueen, I.A. Troyan, T. Palasyuk, M.I. Eremets, R.J. Cava, S. Naghavi, F. Casper, V. Ksenofontov, G. Wortmann, C. Felser, Electronic and magnetic phase diagram of beta-Fe(1.01)Se with superconductivity at 36.7 K under pressure, Nature Mater. 8 (2009) 630–633.
[14] A.I. Coldea, J.D. Fletcher, A. Carrington, J.G. Analytis, A.F. Bangura, J.-H. Chu, A.S. Erickson, I.R. Fisher, N.E. Hussey, R.D. McDonald, Fermi surface of superconducting LaFePO determined from quantum oscillations, Phys. Rev. Lett. 101 (2008) 216402.
[15] M.D. Johannes, I.I. Mazin, Microscopic origin of magnetism and magnetic interactions in ferropnictides, Phys. Rev. B 79 (2009) 220510.
[16] I.I. Mazin, D.J. Singh, M.D. Johannes, M.H. Du, Unconventional superconductivity with a sign reversal in the order parameter of $LaFeAsO_{1-x}F_x$, Phys. Rev. Lett. 101 (2008) 057003.
[17] K. Kuroki, S. Onari, R. Arita, H. Usui, Y. Tanaka, H. Kontani, H. Aoki, Unconventional pairing originating from the disconnected Fermi surfaces of superconducting $LaFeAsO_{1-x}F_x$, Phys. Rev. Lett. 101 (2008) 087004.
[18] A.V. Chubukov, D.V. Efremov, I. Eremin, Magnetism, superconductivity, and pairing symmetry in iron-based superconductors, Phys. Rev. B 78 (2008) 134512.
[19] V. Cvetkovic, Z. Tesanovic, Multiband magnetism and superconductivity in Fe-based compounds, EPL 85 (2009) 37002.
[20] S. Graser, T.A. Maier, P.J. Hirschfeld, D.J. Scalapino, Near-degeneracy of several pairing channels in multiorbital models for the Fe pnictides, New J. Phys. 11 (2009) 025016.
[21] A.V. Chubukov, M.G. Vavilov, A.B. Vorontsov, Momentum dependence and nodes of the superconducting gap in the iron pnictides, Phys. Rev. B 80 (2009) 140515.
[22] K. Kuroki, H. Usui, S. Onari, R. Arita, H. Aoki, Pnictogen height as a possible switch between high-T_c nodeless and low-T_c nodal pairings in the iron-based superconductors, Phys. Rev. B 79 (2009) 224511.
[23] K. Suzuki, H. Usui, K. Kuroki, Possible three dimensional nodes in the $s\pm$ superconducting gap of $BaFe_2(As_{1-x}P_x)_2$, J. Phys. Soc. Jpn. 80 (2011) 013710.
[24] A. Carrington, Studies of the gap structure of iron-based superconductors using magnetic penetration depth, C. R. Phys. 12 (2011) 502–514.
[25] K. Hashimoto, S. Kasahara, R. Katsumata, Y. Mizukami, M. Yamashita, H. Ikeda, T. Terashima, A. Carrington, Y. Matsuda, T. Shibauchi, Nodal versus nodeless behaviors of the order parameters of LiFeP and LiFeAs superconductors from magnetic penetration-depth measurements, Phys. Rev. Lett. 108 (2012) 047003.
[26] M. Kano, Y. Kohama, D. Graf, F. Balakirev, A. Sefat, M. Mcguire, B. Sales, D. Mandrus, S. Tozer, Anisotropy of the upper critical field in a Co-doped $BaFe_2As_2$ single crystal, J. Phys. Soc. Jpn. 78 (2009) 084719.
[27] D. Braithwaite, G. Lapertot, W. Knafo, I. Sheikin, Evidence for anisotropic vortex dynamics and Pauli limitation in the upper critical field of $FeSe_{1-x}Te_x$, J. Phys. Soc. Jpn. 79 (2010) 053703.
[28] T. Klein, D. Braithwaite, A. Demuer, W. Knafo, G. Lapertot, C. Marcenat, P. Rodiere, I. Sheikin, P. Strobel, A. Sulpice, P. Toulemonde, Thermodynamic phase diagram of $FeSe_{0.5}Te_{0.5}$ single crystals in fields up to 28 Tesla, Phys. Rev. B 82 (2010) 184506.
[29] M. Putti, I. Pallecchi, E. Bellingeri, M.R. Cimberle, M. Tropeano, C. Ferdeghini, A. Palenzona, C. Tarantini, A. Yamamoto, J. Jiang, J. Jaroszynski, F. Kametani, D. Abraimov, A. Polyanskii, J.D. Weiss, E.E. Hellstrom, A. Gurevich, D.C. Larbalestier, R. Jin, B.C. Sales, A.S. Sefat, M.A. McGuire, D. Mandrus, P. Cheng, Y. Jia, H.H. Wen, S. Lee, C.B. Eom, New Fe-based superconductors: properties relevant for applications, Supercond. Sci. Technol. 23 (2010) 034003.

[30] N. Werthame, E. Helfand, P. Hohenber, Temperature and purity dependence of superconducting critical field H_{c2}. 3. Electron spin and spin–orbit effects, Phys. Rev. 147 (1966) 295.

[31] U. Welp, R. Xie, A.E. Koshelev, W.K. Kwok, P. Cheng, L. Fang, H.H. Wen, Calorimetric determination of the upper critical fields and anisotropy of $NdFeAsO_{1-x}F_x$ single crystals, Phys. Rev. B 78 (2008) 140510.

[32] Z. Pribulova, T. Klein, J. Kacmarcik, C. Marcenat, M. Konczykowski, S.L. Bud'ko, M. Tillman, P.C. Canfield, Upper and lower critical magnetic fields of superconducting $ndfeaso_{1-x}f_x$ single crystals studied by hall-probe magnetization and specific heat, Phys. Rev. B 79 (2009) 020508.

[33] U. Welp, G. Mu, R. Xie, A.E. Koshelev, W.K. Kwok, H.Q. Luo, Z.S. Wang, P. Cheng, L. Fang, C. Ren, H.H. Wen, Specific heat and phase diagrams of single crystal iron pnictide superconductors, Physica C 69 (2009) 575–581.

[34] H.Q. Yuan, J. Singleton, F.F. Balakirev, S.A. Baily, G.F. Chen, J.L. Luo, N.L. Wang, Nearly isotropic superconductivity in $(Ba,K)Fe_2As_2$, Nature 457 (2009) 565–568.

[35] A. Serafin, A.I. Coldea, A.Y. Ganin, M.J. Rosseinsky, K. Prassides, D. Vignolles, A. Carrington, Anisotropic fluctuations and quasiparticle excitations in $FeSe_{0.5}Te_{0.5}$, Phys. Rev. B 82 (2010) 104514.

[36] Y. Kohama, C. Marcenat, T. Klein, M. Jaime, AC measurement of heat capacity and magnetocaloric effect for pulsed magnetic fields, Rev. Sci. Inst. 81 (2010) 104902.

[37] F. Hunte, J. Jaroszynski, A. Gurevich, D.C. Larbalestier, R. Jin, A.S. Sefat, M.A. McGuire, B.C. Sales, D.K. Christen, D. Mandrus, Two-band superconductivity in $LaFeAsO_{0.89}F_{0.11}$ at very high magnetic fields, Nature 453 (2008) 903–905.

[38] G. Fuchs, S.-L. Drechsler, N. Kozlova, M. Bartkowiak, J.E. Hamann-Borrero, G. Behr, K. Nenkov, H.-H. Klauss, H. Maeter, A. Amato, H. Luetkens, A. Kwadrin, R. Khasanov, J. Freudenberger, A. Köhler, M. Knupfer, E. Arushanov, H. Rosner, B. Büchner, L. Schultz, Orbital and spin effects for the upper critical field in As-deficient disordered Fe pnictide superconductors, New J. Phys. 11 (2009) 075007.

[39] S.A. Baily, Y. Kohama, H. Hiramatsu, B. Maiorov, F.F. Balakirev, M. Hirano, H. Hosono, Pseudoisotropic upper critical field in cobalt-doped $SrFe_2As_2$ epitaxial films, Phys. Rev. Lett. 102 (2009) 117004.

[40] L. Jiao, J.L. Zhang, F.F. Balakirev, G.F. Chen, J.L. Luo, N.L. Wang, H.Q. Yuan, Upper critical field of the 122-type iron pnictide superconductors, J. Phys. Chem. Solids 72 (2011) 423–425.

[41] A. Tamai, A.Y. Ganin, E. Rozbicki, J. Bacsa, W. Meevasana, P.D.C. King, M. Caffio, R. Schaub, S. Margadonna, K. Prassides, M.J. Rosseinsky, F. Baumberger, Strong electron correlations in the normal state of the iron-based $FeSe_{0.42}Te_{0.58}$ superconductor observed by angle-resolved photoemission spectroscopy, Phys. Rev. Lett. 104 (2010) 097002.

[42] Seunghyun Khim, Jun Sung Kim, Jae Wook Kim, Suk Ho Lee, F. Balakirev, Yunkyu Bang, Kee Hoon Kim, Nearly isotropic upper critical fields in a $SrFe_{1.85}Co_{0.15}As_2$ single crystal, Physica C (2010) S317–S319.

[43] Hechang Lei, Rongwei Hu, E. Choi, J. Warren, C. Petrovic, Pauli-limited upper critical field of $Fe_{1+y}Te_{1-x}Se_x$, Phys. Rev. B 81 (2010) 094518.

[44] S. Khim, B. Lee, J.W. Kim, E.S. Choi, G.R. Stewart, K.H. Kim, Pauli-limiting effects in the upper critical fields of a clean LiFeAs single crystal, Phys. Rev. B 84 (2011) 104502.

[45] V.A. Gasparov, L. Drigo, A. Audouard, D.L. Sun, C.T. Lin, S.L. Bud'ko, P.C. Canfield, F.W. Fabris, J. Wosnitza, Upper critical magnetic field in $Ba_{0.68}K_{0.32}Fe_2As_2$ and $Ba(Fe_{0.93}Co_{0.07})_2As_2$, JETP Lett. 93 (2011) 667–672.

[46] N. Hussey, M. Abdel-Jawad, A. Carrington, A. Mackenzie, L. Balicas, A coherent three-dimensional Fermi surface in a high-transition-temperature superconductor, Nature 425 (2003) 814–817.

[47] M. Abdel-Jawad, M.P. Kennett, L. Balicas, A. Carrington, A.P. Mackenzie, R.H. McKenzie, N.E. Hussey, Anisotropic scattering and anomalous normal-state transport in a high-temperature superconductor, Nature Phys. 2 (2006) 821–825.

[48] M. Abdel-Jawad, J.G. Analytis, L. Balicas, A. Carrington, J.P.H. Charmant, M.M.J. French, N.E. Hussey, Correlation between the superconducting transition temperature and anisotropic quasiparticle scattering in $Tl_2Ba_2CuO_{6+\delta}$, Phys. Rev. Lett. 99 (2007) 107002.

[49] S. Blundell, J. Singleton, Angle-dependent magnetoresistance in organic metals, J. Phys. I 6 (1996) 1837–1847.

[50] M. Kimata, T. Terashima, N. Kurita, H. Satsukawa, A. Harada, K. Kodama, A. Sato, M. Imai, K. Kihou, C.H. Lee, H. Kito, H. Eisaki, A. Iyo, T. Saito, H. Fukazawa, Y. Kohori, H. Harima, S. Uji, Quasi-two-dimensional Fermi surfaces and coherent interlayer transport in KFe(2)As(2), Phys. Rev. Lett. 105 (2010) 246403.

[51] K. Yamaji, On the angle dependence of the magnetoresistance in quasi-2-dimensional organic superconductors, J. Phys. Soc. Jpn. 58 (1989) 1520.

[52] Brendan Arnold, Ph.D. thesis, University of Bristol, 2012.

[53] B.J. Arnold, S. Kasahara, A.I. Coldea, T. Terashima, Y. Matsuda, T. Shibauchi, A. Carrington, Nesting of electron and hole Fermi surfaces in nonsuperconducting $BaFe_2P_2$, Phys. Rev. B 83 (2011) 220504.

[54] J.G. Analytis, C.M.J. Andrew, A.I. Coldea, A. McCollam, J.-H. Chu, R.D. McDonald, I.R. Fisher, A. Carrington, Fermi surface of $SrFe_2P_2$ determined by the de Haas–van Alphen effect, Phys. Rev. Lett. 103 (2009) 076401.

[55] A.I. Coldea, C.M.J. Andrew, J.G. Analytis, R.D. McDonald, A.F. Bangura, J.-H. Chu, I.R. Fisher, A. Carrington, Topological change of the Fermi surface in ternary iron pnictides with reduced c/a ratio: A de Haas–van Alphen study of $CaFe_2P_2$, Phys. Rev. Lett. 103 (2009) 026404.

[56] M. Yi, D.H. Lu, J.G. Analytis, J.-H. Chu, S.-K. Mo, R.-H. He, M. Hashimoto, R.G. Moore, I.I. Mazin, D.J. Singh, Z. Hussain, I.R. Fisher, Z.-X. Shen, Unconventional electronic reconstruction in undoped $(Ba,Sr)Fe_2As_2$ across the spin density wave transition, Phys. Rev. B 80 (2009) 174510.

[57] J.G. Analytis, R.D. Mcdonald, J.H. Chu, S.C. Riggs, A.F. Bangura, C. Kucharczyk, M. Johannes, I.R. Fisher, Quantum oscillations in the parent pnictide $BaFe_2As_2$: Itinerant electrons in the reconstructed state, Phys. Rev. B 80 (2009) 064507.

[58] T. Terashima, N. Kurita, M. Tomita, K. Kihou, C.-H. Lee, Y. Tomioka, T. Ito, A. Iyo, H. Eisaki, T. Liang, M. Nakajima, S. Ishida, S.-i. Uchida, H. Harima, S. Uji, Complete Fermi surface in $BaFe_2As_2$ observed via Shubnikov–de Haas oscillation measurements on detwinned single crystals, Phys. Rev. Lett. 107 (2011) 176402.

[59] S.E. Sebastian, J. Gillett, N. Harrison, P.H.C. Lau, D.J. Singh, C.H. Mielke, G.G. Lonzarich, Quantum oscillations in the parent magnetic phase of an iron arsenide high temperature superconductor, J. Phys. Condens. Matter. 20 (2008) 422203.

[60] N. Harrison, R.D. Mcdonald, C.H. Mielke, E.D. Bauer, F. Ronning, J.D. Thompson, Quantum oscillations in antiferromagnetic $CaFe_2As_2$ on the brink of superconductivity, J. Phys. Condens. Matter. 21 (2009) 322202.

[61] L. Boeri, O.V. Dolgov, A.A. Golubov, Electron–phonon properties of pnictide superconductors, Physica C 469 (2009) 628–634.

[62] H. Takahashi, K. Ando, Y. Shirakawabe, Self-sensing piezoresistive cantilever and its magnetic force microscopy applications, Ultramicroscopy 91 (2002) 63–72.

[63] L. Ortenzi, E. Cappelluti, L. Benfatto, L. Pietronero, Fermi-surface shrinking and interband coupling in iron-based pnictides, Phys. Rev. Lett. 103 (2009) 046404.

[64] C. Putzke, A.I. Coldea, I. Guillamón, D. Vignolles, A. McCollam, D. LeBoeuf, M.D. Watson, I.I. Mazin, S. Kasahara, T. Terashima, T. Shibauchi, Y. Matsuda, A. Carrington, de Haas–van Alphen study of the Fermi surfaces of superconducting LiFeP and LiFeAs, Phys. Rev. Lett. 108 (2012) 047002.

[65] H. Shishido, A.F. Bangura, A.I. Coldea, S. Tonegawa, K. Hashimoto, S. Kasahara, P.M.C. Rourke, H. Ikeda, T. Terashima, R. Settai, Y. Onuki, D. Vignolles, C. Proust, B. Vignolle, A. McCollam, Y. Matsuda, T. Shibauchi, A. Carrington, Evolution of the Fermi surface of $BaFe_2(As_{1-x}P_x)_2$ on entering the superconducting dome, Phys. Rev. Lett. 104 (2010) 057008.

[66] H. Sugawara, R. Settai, Y. Doi, H. Muranaka, K. Katayama, H. Yamagami, Y. Onuki, de Haas–van Alphen effect in LaFePO with two-dimensional cylindrical Fermi surfaces, J. Phys. Soc. Jpn. 77 (2008) 113711.

[67] I.R. Shein, A.L. Ivanovskii, Electronic properties of novel 6 K superconductor LiFeP in comparison with LiFeAs from first principles calculations, Solid State Commun. 150 (2010) 152–156.
[68] J.G. Analytis, J.-H. Chu, R.D. McDonald, S.C. Riggs, I.R. Fisher, Enhanced Fermi-surface nesting in superconducting $BaFe_2(As_{1-x}P_x)_2$ revealed by the de Haas–van Alphen effect, Phys. Rev. Lett. 105 (2010) 207004.
[69] H. Shishido, R. Settai, H. Harima, Y. Onuki, A drastic change of the Fermi surface at a critical pressure in CeRhIn5: dHvA study under pressure, J. Phys. Soc. Jpn. 74 (2005) 1103–1106.
[70] T. Yoshida, I. Nishi, S. Ideta, A. Fujimori, M. Kubota, K. Ono, S. Kasahara, T. Shibauchi, T. Terashima, Y. Matsuda, H. Ikeda, R. Arita, Two-dimensional and three-dimensional Fermi surfaces of superconducting $BaFe_2(As_{1-x}P_x)_2$ and their nesting properties revealed by angle-resolved photoemission spectroscopy, Phys. Rev. Lett. 106 (2011) 117001.